ACS central science

Research Article

http://pubs.acs.org/journal/acscii

Mechanical Response of DNA−Nanoparticle Crystals to Controlled Deformation

Joshua Lequieu,[†] Andrés Córdoba,[†] Daniel Hinckley,[‡] and Juan J. de Pablo*[,†,§]

[†]Institute for Molecular Engineering, University of Chicago, Chicago, Illinois 60637, United States

[‡]Department of Chemical and Biological Engineering, University of Wisconsin—Madison, Madison, Wisconsin 53706, United States

[§]Materials Science Division, Argonne National Laboratory, Argonne, Illinois 60439, United States

Supporting Information

ABSTRACT: The self-assembly of DNA-conjugated nanoparticles represents a promising avenue toward the design of engineered hierarchical materials. By using DNA to encode nanoscale interactions, macroscale crystals can be formed with mechanical properties that can, at least in principle, be tuned. Here we present *in silico* evidence that the mechanical response of these assemblies can indeed be controlled, and that subtle modifications of the linking DNA sequences can change the Young's modulus from 97 kPa to 2.1 MPa. We rely on a detailed molecular model to quantify the energetics of DNA−nanoparticle assembly and demonstrate that the mechanical response is governed by entropic, rather than enthalpic, contributions and that the response of the entire network can be estimated from the elastic properties of an individual nanoparticle. The results here provide a first step toward the mechanical characterization of DNA−nanoparticle assemblies, and suggest the possibility of mechanical metamaterials constructed using DNA.

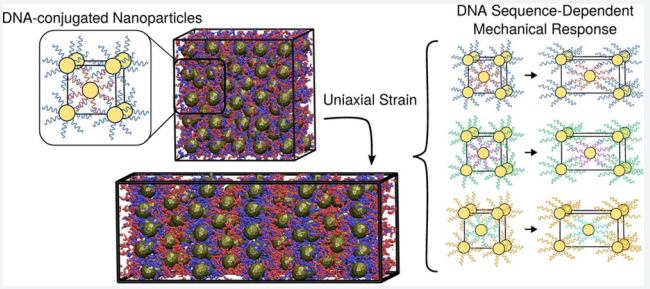

INTRODUCTION

Nanoparticles functionalized with short sequences of DNA represent a highly customizable platform for multiscale materials design. In such systems, interactions between nanoparticles are mediated by short strands of DNA, typically with lengths on the order of tens of base pairs.[1,2] By varying the length and composition of these linking DNA sequences, the strength, range, and specificity of interparticle interactions can be precisely tuned. The ability to customize and specify DNA-mediated interactions promises to facilitate the design of hierarchical structures whose macroscopic properties could be tuned by manipulating the corresponding nanoscale building blocks of which they are composed.

DNA-functionalized nanoparticles have now been shown to assemble into crystals with long-range order[3,4] that possess tunable lattice parameters and crystal symmetries based on DNA sequence alone.[5] Through advances in nanoscale synthesis, it has also become possible to assemble nanoparticles of different shapes and properties.[6−9] The resulting materials exhibit intriguing properties, such as dynamic reprogramming[10] and single crystal assembly with well-defined facets,[11] and have been predicted to demonstrate re-entrant melting.[12] Recent work has demonstrated that DNA-programmed assemblies have useful, tunable plasmonic properties.[13−16] A largely underexplored aspect of DNA-functionalized nanoparticle assemblies, however, is related to the tunability of their mechanical properties. Though two-dimensional films of DNA-functionalized nanoparticles have been assembled[17] and shown to have extraordinary mechanical properties,[18] little work[19] has been done to characterize or tune the mechanics of DNA−nanoparticle assemblies, especially in three dimensions.

Our interest in mechanically tunable DNA−nanoparticle assemblies builds on recent work examining the mechanical response of nanoparticles conjugated with other short organic ligands. Extremely strong, two-dimensional nanoparticle sheets have been prepared with nanoparticles functionalized with simple dodecanethiol ligands.[20−22] At the other end of the chain-length spectrum, Williams et al.[23] have shown that polymer-grafted nanoparticles interacting via hydrogen bonds assemble into a fcc crystal with a Young's modulus of 26−82 MPa that is capable of self-healing.[23] Importantly, these authors demonstrated that the mechanical and optical response can be tuned by varying the length of polymer grafts, and that the optical properties can be altered by mechanical deformation. More generally, the mechanical properties of ligand-conjugated nanoparticle assemblies are of fundamental interest because they arise from nonlinear combinations of their constituents; indeed, they possess characteristics of both granular (due to the nanoparticles) and viscoelastic (due to the ligands) systems.[24]

In this work, we present a first step toward the detailed characterization of the mechanical response of DNA−nanoparticle assemblies. To achieve this, we rely on a detailed molecular model to examine the mechanical properties of

Received: June 10, 2016
Published: August 17, 2016

DOI: 10.1021/acscentsci.6b00170
ACS Cent. Sci. 2016, 2, 614−620

DNA-conjugated nanoparticle assemblies *in silico*. Our results demonstrate that such properties can indeed be tuned by using different DNA sequences, DNA loading densities, and temperature, thereby providing a potentially useful platform for the creation of mechanical metamaterials.

RESULTS AND DISCUSSION

Mechanical Response of DNA-Conjugated Nanoparticle Lattices. DNA-conjugated nanoparticle lattices were assembled as described in Methods, and their mechanical response was measured under uniaxial extension (Figure 1).

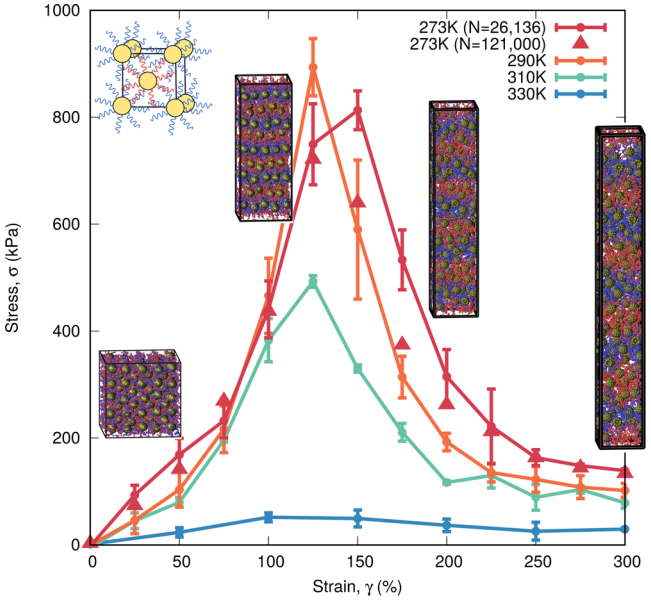

Figure 1. Stress–strain response of DNA–nanoparticle assembly under uniaxial extension for sequence B (see Figure 2). Simulation snapshots show the material after 0%, 100%, 200%, and 300% strain. All DNA sequences of the same type are given the same color (i.e., red or blue). Error bars denote a standard deviation over three independently initialized nanoparticle assemblies.

The deformation was applied quasi-statically, where a nanoparticle assembly was deformed to the specified strain and then held fixed until the stress re-equilibrated. The resulting stress–strain curve exhibits elasticity (i.e., linear response) for all temperatures up to strains of 50%. Following this elastic regime, the material stiffens until its peak stress at ≈125–150% strain.

At strains above the peak stress, the material does not immediately yield, but instead the stress decreases slowly: even at strains of 300% there is still a small but nonzero stress. Notably, even at these large strains, the material does not exhibit necking and is characterized by constant densities throughout the sample (Figure 1 snapshots, Figure S2). Yet despite the lack of macroscopic defects (i.e., necking), the microscopic structure of the nanoparticle assembly is significantly perturbed under large strains. For deformations beyond the peak stress, the long-range crystalline order within the nanoparticle network is disrupted, and the assemblies become amorphous (Figure 1 snapshots, Figures S3 and S4). This observation suggests that, under sufficiently slow deformation (i.e., quasi-static), the microstructure of the assembly can rearrange, thereby preventing the formation of failure-prone morphologies, including necks or voids. This behavior can be thought of as a form of microscopic self-healing, where individual nanoparticles reposition themselves within the network to maintain the integrity of the material.

Temperature also plays an important role in the mechanical response (Figure 1). Though the material exhibits a response in the kPa range at low temperatures, higher temperatures result in material softening and, eventually, a negligible mechanical response (e.g., 330 K). The extreme softening of the material occurs for this assembly between 310 and 330 K, corresponding extremely well to the 310–315 K melting temperature of this DNA sequence calculated previously.[25]

In order to confirm that our measurements are representative of a bulk material and do not suffer from finite-size effects, simulations were also performed for systems consisting of 125 bcc unit cells, corresponding to 121,000 total coarse-grained sites (Figure 1, red triangles). The results from this larger system are largely indistinguishable from those of the 27 unit cell assembly (N = 26,136), confirming that our simulations are representative of a bulk material. Accordingly, nanoparticle assemblies consisting of 27 unit cells will be used throughout the remainder of this work.

Tunable Sequence-Dependent Mechanical Response. A potential feature of DNA–nanoparticle assemblies is that subtle changes in the linking DNA sequences may be used to generate materials with different properties. To examine the effect of DNA sequence on the mechanical response, we repeated our analysis above using different DNA sequences (Figure 2). Because the parameter space corresponding to all

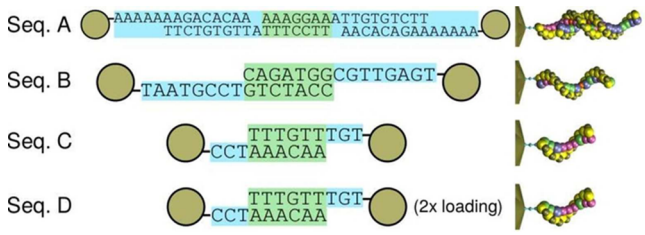

Figure 2. Different DNA sequences conjugated to nanoparticle surface. Green highlights the complementary "sticky end" region, while blue highlights the nonreactive "linker" region. Snapshots corresponding to the molecular topology of each DNA linker are shown. "2× loading" denotes that Seq D contains twice the number of DNA strands per nanoparticle. Note that Seq A's linker consists of two DNA strands and contains a nonreactive double-stranded region, while the linkers of Seq B, C, and D consist of only a single DNA strand.

possible DNA sequences is prohibitively large, we focused here on a subset of DNA parameters that have been varied elsewhere in the DNA–nanoparticle literature.[4,5,25,26] These include the effect of "one strand" vs "two strand" linkers (i.e., Seq A vs Seq B), the effect of linker length (Seq A vs Seq C), the effect of DNA loading density (Seq C vs Seq D), and the effect of the complementary DNA "sticky ends" (Seq A vs Seq B vs Seq C and D). Consistent with experimental systems,[3,11,27] the sequences chosen here contain complementary "sticky" DNA regions of 6–7 base pairs.

The mechanical response is shown to be dramatically dependent on DNA sequence (Figure 3). One sequence-dependent effect is the qualitative difference in mechanical response between sequences with short linkers (i.e., C and D) relative to sequences with long linkers (i.e., A and B). Sequences C and D demonstrate a stiff initial response ($E \approx$ 700–2100 kPa) but exhibit little strain hardening, and lose nearly all stiffness at strains greater than 100%. In contrast,

DOI: 10.1021/acscentsci.6b00170
ACS Cent. Sci. 2016, 2, 614–620

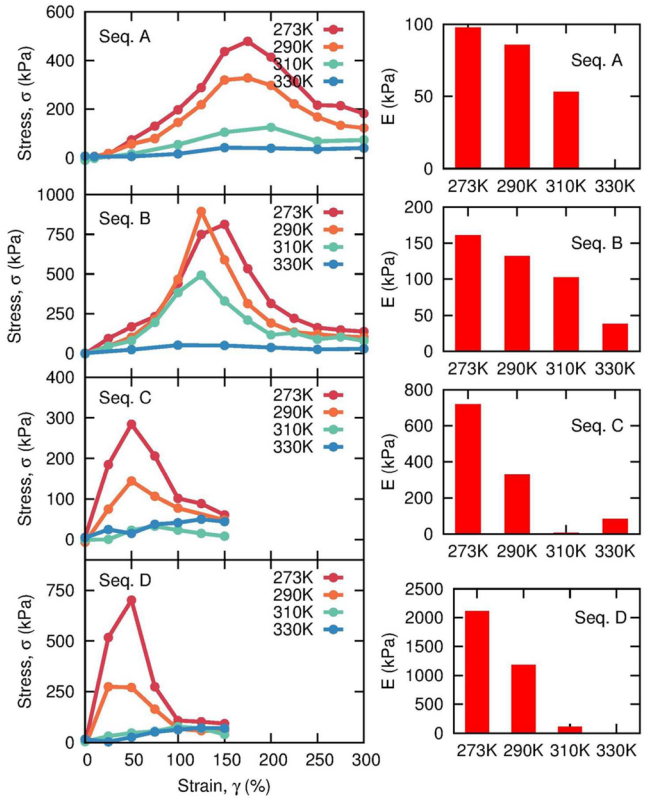

Figure 3. DNA sequence-dependent mechanical response. Stress–strain response of sequences A, B, C, and D and corresponding Young's modulus, E, at different temperatures. Variations in both temperature and sequence result in both qualitative and quantitative changes in the stress–strain response of DNA–nanoparticle assemblies.

sequences A and B exhibit a softer initial response ($E \approx 100$ kPa) but a large peak strain (≈500–750 kPa). Additionally, long linkers enable strains of up to 300% without mechanical rupture. Thus, short linkers give rise to "brittle" mechanical behavior, while longer linkers result in more pliable materials. Curiously, though sequence A and sequence B are formed from very different linker types (i.e., double-stranded vs single-stranded), they nonetheless demonstrate a qualitatively similar mechanical response. Though double-stranded linkers are stiff, the similarities between our results for Seq A and Seq B suggests that the mechanical response is predominantly driven by the single-stranded linker of the assemblies constructed using sequence A. This result suggests that it is not the type of DNA linker but rather its single-stranded length that dictates the mechanical response of DNA-nanoparticle assemblies.

The effect of DNA coverage can be assessed by comparing sequences C and D. Assemblies using these linkers use identical DNA sequences and differ only in the density (i.e., loading) of DNA strands conjugated to the nanoparticle surface. That is, Seq D has twice the number of DNA strands on the nanoparticle surface relative to Seq C. Our results demonstrate that DNA loading density results in significant changes to the stress–strain response. For example, by simply doubling the DNA loading (i.e., nine strands for Seq C vs 18 strands for Seq D), the Young's modulus changes by a factor of 3 (≈700 kPa to ≈2100 kPa) and the peak stress more than doubles (≈300 kPa to ≈740 kPa). Yet, despite these changes, the qualitative features of the mechanical responses of Seq C and D remain largely unchanged: the stress increases linearly up until a peak strain at $\gamma \approx 50\%$ and then decreases significantly. This result suggests that DNA loading represents an important parameter for tuning mechanical behavior. Whereas the qualitative features of the mechanical response can be adjusted by changing the characteristics of the DNA sequences themselves, the magnitude of the response can be adjusted independently by varying the DNA loading on the nanoparticle surface. In that sense, DNA coverage represents a system parameter orthogonal to the DNA sequence itself, which can be tuned to obtain the desired mechanical response. Additionally, since the number of strands increases approximately with the square of the nanoparticle radius, the larger 10–20 nm nanoparticles used experimentally[3,4,11] will possess even more particle–particle connections and likely a significanlty stronger mechanical response.

Interestingly, the different DNA sequences studied here exhibit different temperature-dependent mechanical properties. The mechanical response of Seq B is nearly unchanged between 273 and 290 K, for example, while those of sequences C and D over this same temperature range change dramatically. These different behaviors can be explained in terms of the melting temperature, T_m, of the DNA "sticky ends" that link complementary particles. By choosing "sticky ends" with a higher T_m (as with Seq B), the nanoparticles demonstrate higher thermal stability and are more mechanically robust. Because DNA–nanoparticles are known to exhibit extremely sharp melting curves,[28] our results here suggest the possibility of extremely sensitive thermoresponsive materials whose mechanical properties could change by orders of magnitude with temperature changes of only several degrees.

Molecular Origin of Mechanical Response. Having considered the mechanical properties of DNA–nanoparticle assemblies, we now turn our attention to the molecular processes responsible for specific sequence-dependent mechanical responses. Specifically, we seek to provide a molecular explanation of the stress–strain curves reported in Figure 3. In particular, we will examine whether the mechanical response correlates more strongly with (a) the enthalpic penalty arising from the disruption of base pairs or (b) the entropic penalty arising from the anisotropic ordering of DNA strands on the nanoparticle surface.

Since nanoparticle–nanoparticle interactions are mediated by complementary DNA–DNA base pairs, deformation of the network is expected to result in base pair disruption. Disruption of base pairs will incur an enthalpic penalty, and therefore we anticipate that disruption of base pairs might correlate strongly with the observed stress–strain response. Figure 4a shows the network connectivity (expressed as the number of base pairs in the network) for each DNA sequence as a function of strain. As expected, strain disrupts the DNA–nanoparticle network, and the number of base pairs is observed to decrease. Notably, the slope of the base pair–strain curve (i.e., the derivative) differs between different DNA sequences. For short DNA linkers (i.e., sequences C and D), the decrease in base pairs is more rapid than for DNA–nanoparticles with longer linkers (sequences A and B). The slope of the base pair–strain curve is quantified by calculating the numerical derivative shown in the bottom panel of Figure 4a. Sequences C and D demonstrate a sharply peaked derivative at 50% strain, corresponding to the maximum in their respective stress–strain response (Figure 3). This correlation suggests that the stress–strain response is influenced by the rate of base pair disruption and the associated enthalpic penalty.

DOI: 10.1021/acscentsci.6b00170
ACS Cent. Sci. 2016, 2, 614–620

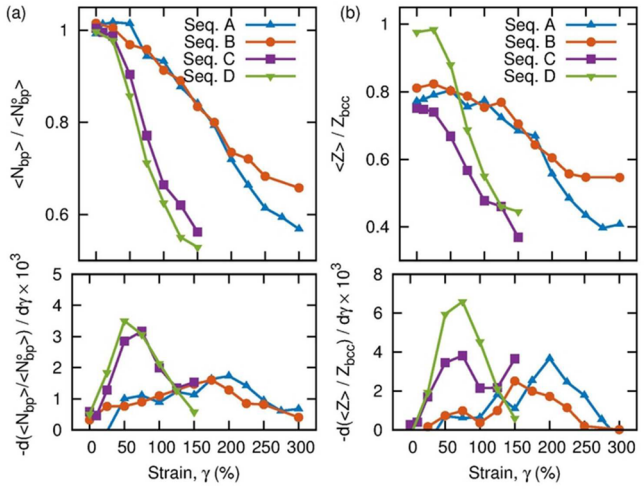

Figure 4. Effect of deformation on connectivity of DNA–nanoparticle network. (a) Average number of base pairs, $\langle N_{bp} \rangle$, and numerical derivative, $\frac{d\langle N_{bp} \rangle}{d\gamma}$, and (b) average coordination number, $\langle Z \rangle$, and numerical derivative, $\frac{d\langle Z \rangle}{d\gamma}$, for different DNA–nanoparticle sequences at 273 K. Though the disruption of base pairs influences the mechanical behavior, analysis of network connectivity alone is insufficient to fully explain the mechanical response.

This possibility, however, is only weakly supported by the results for sequences A and B. For these two sequences, the derivatives are approximately independent of strain and show only a subtle peak at 175%–200% strain, a value higher than the peak in the stress–strain response at 125%–175%. Therefore, though the disruption of base pairs influences the mechanical behavior, our results suggest that it is not the predominant explanation for the observed sequence-dependent mechanical response.

A notable feature of Figure 4a is that the number of base pairs does not decrease to zero. Even after the assembly has been mechanically disrupted, 60% to 70% of the original base pairs are still intact. This observation led us to propose that it is not the absolute number of base pairs that matters for the mechanical response, but it is instead the connectivity of the network. To test this hypothesis, we measure the connectivity of the network on the basis of nanoparticle coordination number. In this context, we define the coordination number, Z, as the number of neighboring nanoparticles that a given nanoparticle is base paired to, normalized by that expected in a bcc crystal lattice, $Z_{bcc} = 8$, (Figure 4b). At rest, sequences with ordinary DNA loading densities (sequences A, B, C) have coordination numbers that are ≈80% of the ideal value. This result is expected since these particles contain only nine DNA strands per particle, and therefore the probability of forming DNA "bonds" between all 8 bcc neighbors is small. However, for particles with a higher loading density (Seq D), the connectivity of the network is essentially complete, with $Z/Z_{bcc} \approx 1.0$ at 0% strain. The near perfect connectivity of sequence D helps explain its high mechanical strength: as the connectivity approaches the ideal value, mechanical properties increase considerably. Note, however, that our analysis of the coordination number is still insufficient to completely explain the sequence-dependent stress–strain response. As with the number of base pairs, N_{bp}, shown in Figure 4a, the coordination number in Figure 4b decreases with strain and the derivative (lower panel) correlates weekly with the stress–strain curves.

Another possible explanation for the role of sequence on mechanical properties relates the deformation of individual DNA-conjugated nanoparticles themselves to the overall deformation of the network. During network deformation, it might be expected that the DNA strands conjugated to the nanoparticle surface would anisotropically orient themselves along the direction of the applied strain. Such ordering would incur an entropic penalty and could be responsible for the observed sequence-dependent mechanical response. Indeed, such entropic penalties dominate the mechanical properties of polymer melts, and could be significant in DNA–nanoparticle assemblies as well.

To examine the role of this entropic ordering, the shape of individual nanoparticles was quantified by calculating the radius of gyration tensor, $S_{\alpha\beta}$, for each DNA-conjugated nanoparticle, and then determining its three eigenvalues, $\lambda_1 > \lambda_2 > \lambda_3$. The ratio of the two largest eigenvalues, λ_1/λ_2, gives the anisotropic shape of each nanoparticle with $\lambda_1/\lambda_2 \approx 1$ representing a sphere and $\lambda_1/\lambda_2 \to \infty$ an infinite rod.[29] Since the nanoparticles are very rigid, values of $\lambda_1/\lambda_2 \neq 1$ represent deformations of the conjugated DNA strands, and not the nanoparticles themselves (Figure 5a, graphic). We will refer to λ_1/λ_2 as the "anisotropy" of the DNA–nanoparticles.

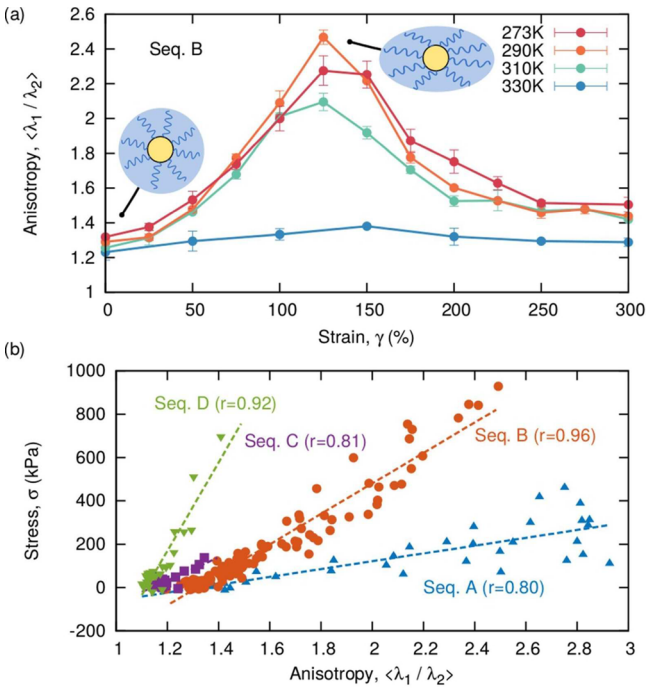

Figure 5. Anisotropic deformation of individual nanoparticle shape. (a) Average anisotropy of DNA–nanoparticle shape during deformation. The anisotropy is qualitatively similar to the mechanical response (cf. Figure 1). (b) Correlation between DNA–nanoparticle anisotropy and calculated stress during deformation. For all sequences and temperatures, a strong correlation exists.

The average anisotropy for different values of strain and temperature is shown in Figure 5a for sequence B. At zero strain, the anisotropy is small and the individual DNA–nanoparticles are nearly spherical, as expected. As strain is increased, the average anisotropy increases up to a peak at 125% and then decays toward its initial value for strains of up to

DOI: 10.1021/acscentsci.6b00170
ACS Cent. Sci. 2016, 2, 614–620

300%. The anisotropy is also temperature dependent; higher temperatures lead to less anisotropy. The most important feature of this result, however, is the striking similarity between the anisotropy and the stress (cf. Figure 1). In fact, both curves appear to be qualitatively identical, with the same maximum, curvature, and temperature dependence. This observation suggests that the shape anisotropy and the stress might be fundamentally related within the DNA−nanoparticle network.

To quantify this relationship, the correlation between anisotropy and stress was calculated for all sequences and temperatures used in this study (Figure 5b). Confirming the previous observation for sequence B, a strong correlation ($0.8 < r < 0.96$) exists between anisotropy and stress for all DNA sequences considered here. This striking result suggests that strain within the DNA−nanoparticle network is strongly related to the anisotropic deformation of the DNA strands on the particle surface, which gives rise to a free energy penalty that manifests itself as a restoring stress when the network is deformed.

An important feature of Figure 5b is that each DNA sequence exhibits a different relationship between stress and anisotropic deformation; or in other words, each DNA sequence shows a different slope. The softest assembly examined here, sequence A, has the smallest slope (i.e., low stress per anisotropic deformation), whereas increasing assembly stiffness (i.e., Seq D) leads to increasingly large slopes (i.e., high stress per anisotropic deformation). These results suggest that each DNA sequence possesses an inherent property, which we refer to as "shape stiffness", that corresponds to the entropic penalty incurred by causing the DNA strands to order anisotropically. Notably, shape stiffness is sequence dependent: for sequence A, the long DNA linkers incur a relatively small penalty upon ordering, leading to small "shape stiffness". In contrast, the short DNA linkers in sequences C and D give rise to a larger penalty upon ordering, causing the "shape stiffness" to be large. Therefore, our results indicate that the "shape stiffness" of a single DNA−nanoparticle represents a key parameter that dictates the mechanical response of the entire DNA−nanoparticle network.

The importance of "shape stiffness" has several implications for the design of DNA−nanoparticle assemblies. First, our results suggest that by simply quantifying the "shape stiffness" for a single nanoparticle the mechanical response of the network can be estimated. As such, "shape stiffness" might provide a simple metric for screening the high parameter space of different DNA sequences in order to obtain the desired mechanical response. Second, the importance of entropic, rather than enthalpic, contributions to the mechanical response has important implications for tuning the mechanical response of DNA−nanoparticle assemblies. Though previous studies have emphasized the energy scale of the complementary "sticky ends" in dictating DNA−nanoparticle assembly,[30,31] our results indicate that it is instead the properties of the unreactive linker DNA that dominate the mechanical response. This observation raises the intriguing prospect of tuning independently the mechanical response and the underlying crystal structure, leading to the possibility of creating DNA−nanoparticle assemblies with complex and precisely tunable mechanical properties.

CONCLUSIONS

In this work we have used a detailed molecular model of DNA-conjugated nanoparticles to examine the mechanical properties of DNA−nanoparticle assemblies. We demonstrate that this mechanical response is strongly dependent on temperature and suggest the possibility of thermosensitive materials whose mechanical properties could change by orders of magnitude upon temperature changes of only several degrees. The mechanical response is also shown to be strongly dependent on DNA sequence, and subtle changes in the linking DNA can lead to significant changes in the qualitative and quantitative features of the mechanical response. Then, moving beyond existing experiments, we interrogate our molecular model in order to identify the physics that dictates the observed sequence-dependent mechanical response. By analyzing the connectivity of the network, we show that the enthalpic penalty due to base pair disruption partially explains the observed mechanical response. Most importantly, however, we demonstrate that the overall mechanical response of the network is strongly correlated with the deformation of a single DNA-conjugated nanoparticle. From this observation we suggest a new sequence-dependent parameter, which we refer to as "shape stiffness", that can be used to estimate the mechanical response of a nanoparticle network from a single nanoparticle. The results presented here are the first detailed characterization of the mechanical response of DNA−nanoparticle assemblies, and are the first to demonstrate that the mechanical response can be tuned. Consequently, they represent a valuable step toward understanding the mechanical properties of DNA−nanoparticle assemblies and are useful for dictating their future directions and applications.

METHODS

The molecular model of DNA-conjugated nanoparticles adopted here was introduced and validated in previous work.[25] In this model, DNA is represented by 3SPN.2,[32] the latest model in the 3SPN family.[33,34] As a coarse-grained model, 3SPN.2 represents each nucleotide of DNA with three force sites, one at the center of mass of the sugar, phosphate, and base. 3SPN.2 has been parameterized to reproduce the structural (e.g., helix width, major and minor groove widths) and mechanical (e.g., persistence length) properties of double- and single-stranded DNA. Additionally, 3SPN.2 can reproduce the melting temperature of double-stranded DNA and hairpins as a function of sequence and ionic strength,[32] and has been used in detailed studies of the single-stranded to double-stranded DNA transition.[35] The DNA-conjugated nanoparticles considered here are constructed by tethering 3SPN.2 to a coarse-grained nanoparticle consisting of a bonded network of sites placed on the surface of a sphere. This model results in nanoparticle sites that are fixed at their relative locations on the surface of a sphere, and therefore the positions of DNA strands are also fixed and cannot migrate along the particle surface. This model has been used to examine the precise energetics of pairwise DNA−nanoparticle assembly and was shown to reproduce the correct energy scales and temperature dependence of DNA−nanoparticle association.[25] In this work, we use 5 nm diameter nanoparticles covered with a DNA density of 19 pmol/cm^2 (unless otherwise noted) as shown experimentally.[26] This DNA density corresponds to nine DNA strands on a 5 nm diameter nanoparticle, distributed approximately uniformly across the particle surface. When referring to "double DNA loading", the DNA density was increased to 38 pmol/cm^2, corresponding to 18 strands per 5 nm particle.

Several of the DNA sequences considered here (Figure 2, Seq A and B) are chosen to correspond to those used in

DOI: 10.1021/acscentsci.6b00170
ACS Cent. Sci. 2016, 2, 614−620

previous experimental studies.[3,27] As in previous work,[25] the reactive "sticky end" of the DNA sequence (see Figure 2 green box) is chosen to be identical to that of the experiments. The unreactive "linker" region, however, is scaled to account for differences between experimental and simulated particle diameters. The net effect of this scaling has been examined in detail previously.[25]

DNA−nanoparticle lattices were formed using a binary mixture of nanoparticles coated with different DNA sequences. The DNA sequences were chosen so that interactions between nanoparticles with different DNA sequences are attractive, whereas nanoparticles with the same DNA sequence are not. As a result of these attractive and repulsive interactions, binary nanoparticle mixtures assemble experimentally into body centered cubic (bcc) crystal lattices. The protocol used for assembling the bcc lattices in this work is described in the Supporting Information. When applying uniaxial extension, constant strain was imposed in a single dimension while constant stress was imposed in the nonstrained dimensions. To apply the deformation quasi-statically, the desired strain was applied and the resulting stress was measured following equilibration to its new steady state.

Simulations were performed in the NVT or NPT ensemble using a Langevin thermostat and/or a Parrinello−Rahman barostat with damping coefficients of 1 and 20 ps, respectively, and a time step of 20 fs. The Debye−Hückel approximation was used to model the interactions between phosphate sites which carry a charge of −0.6.[32] Simulations were performed by implementing the 3SPN.2 nanoparticle model[25] into the LAMMPS simulation package.[36] The approach described by Thompson et al.[37] was used to calculate the virial contribution to the pressure from 3SPN.2. The stress tensor was calculated as the sum of the kinetic and virial components,

$$\sigma_{\alpha\beta} = \frac{1}{V}\sum_{k}^{N} m_k v_{k,\alpha} v_{k,\beta} + \frac{1}{V}\sum_{k}^{N} F_{k,\alpha} r_{k,\beta} \quad (1)$$

Note that while the kinetic component of the stress was included, its contribution to the stress was observed to be small.

■ ASSOCIATED CONTENT

Supporting Information

The Supporting Information is available free of charge on the ACS Publications website at DOI: 10.1021/acscentsci.6b00170.

Detailed simulation protocol for DNA−nanoparticle crystal formation and analysis of crystal structure during deformation (PDF)

■ AUTHOR INFORMATION

Corresponding Author

*E-mail: depablo@uchicago.edu.

Notes

The authors declare no competing financial interest.

■ ACKNOWLEDGMENTS

This work was performed under the following financial assistance award 70NANB14H012 from U.S. Department of Commerce, National Institute of Standards and Technology as part of the Center for Hierarchical Materials Design (ChiMaD). The development of advanced sampling codes required for free energy calculations is supported by the U.S. Department of Energy, Office of Science, Basic Energy Sciences, Materials Sciences and Engineering Division through the Midwest Integrated Center for Computational Materials (MICCoM). Computational resources were provided by the Midway computing cluster at the University of Chicago. The authors gratefully acknowledge Professor Heinrich Jaeger and Yifan Wang for helpful discussions.

■ REFERENCES

(1) Mirkin, C. A.; Letsinger, R. L.; Mucic, R. C.; Storhoff, J. J. A DNA-based method for rationally assembling nanoparticles into macroscopic materials. *Nature* **1996**, *382*, 607−609.

(2) Alivisatos, A. P.; Johnsson, K. P.; Peng, X.; Wilson, T. E.; Loweth, C. J.; Bruchez, M. P., Jr; Schultz, P. G. Organization of 'nanocrystal molecules' using DNA. *Nature* **1996**, *382*, 609−611.

(3) Park, S. Y.; Lytton-Jean, A. K. R.; Lee, B.; Weigand, S.; Schatz, G. C.; Mirkin, C. A. DNA-programmable nanoparticle crystallization. *Nature* **2008**, *451*, 553−556.

(4) Nykypanchuk, D.; Maye, M. M.; van der Lelie, D.; Gang, O. DNA-guided crystallization of colloidal nanoparticles. *Nature* **2008**, *451*, 549−552.

(5) Macfarlane, R. J.; Lee, B.; Jones, M. R.; Harris, N.; Schatz, G. C.; Mirkin, C. A. Nanoparticle superlattice engineering with DNA. *Science* **2011**, *334*, 204−208.

(6) Jones, M. R.; Macfarlane, R. J.; Lee, B.; Zhang, J.; Young, K. L.; Senesi, A. J.; Mirkin, C. A. DNA-nanoparticle superlattices formed from anisotropic building blocks. *Nat. Mater.* **2010**, *9*, 913−917.

(7) Zhang, Y.; Lu, F.; Yager, K. G.; van der Lelie, D.; Gang, O. A general strategy for the DNA-mediated self-assembly of functional nanoparticles into heterogeneous systems. *Nat. Nanotechnol.* **2013**, *8*, 865−872.

(8) O'Brien, M. N.; Jones, M. R.; Lee, B.; Mirkin, C. A. Anisotropic nanoparticle complementarity in DNA-mediated co-crystallization. *Nat. Mater.* **2015**, *14*, 833−840.

(9) Lu, F.; Yager, K. G.; Zhang, Y.; Xin, H.; Gang, O. Superlattices assembled through shape-induced directional binding. *Nat. Commun.* **2015**, *6*, 6912.

(10) Zhang, Y.; Pal, S.; Srinivasan, B.; Vo, T.; Kumar, S.; Gang, O. Selective transformations between nanoparticle superlattices via the reprogramming of DNA-mediated interactions. *Nat. Mater.* **2015**, *14*, 840−847.

(11) Auyeung, E.; Li, T. I. N. G.; Senesi, A. J.; Schmucker, A. L.; Pals, B. C.; de la Cruz, M. O.; Mirkin, C. A. DNA-mediated nanoparticle crystallization into Wulff polyhedra. *Nature* **2014**, *505*, 73−77.

(12) Angioletti-Uberti, S.; Mognetti, B. M.; Frenkel, D. Re-entrant melting as a design principle for DNA-coated colloids. *Nat. Mater.* **2012**, *11*, 518−522.

(13) Tan, S. J.; Campolongo, M. J.; Luo, D.; Cheng, W. Building plasmonic nanostructures with DNA. *Nat. Nanotechnol.* **2011**, *6*, 268−276.

(14) Park, D. J.; Zhang, C.; Ku, J. C.; Zhou, Y.; Schatz, G. C.; Mirkin, C. A. Plasmonic photonic crystals realized through DNA-programmable assembly. *Proc. Natl. Acad. Sci. U. S. A.* **2015**, *112*, 977−981.

(15) Ross, M. B.; Ku, J. C.; Vaccarezza, V. M.; Schatz, G. C.; Mirkin, C. A. Nanoscale form dictates mesoscale function in plasmonic DNA-nanoparticle superlattices. *Nat. Nanotechnol.* **2015**, *10*, 453−458.

(16) Young, K. L.; Ross, M. B.; Blaber, M. G.; Rycenga, M.; Jones, M. R.; Zhang, C.; Senesi, A. J.; Lee, B.; Schatz, G. C.; Mirkin, C. A. Using DNA to design plasmonic metamaterials with tunable optical properties. *Adv. Mater.* **2014**, *26*, 653−659.

(17) Srivastava, S.; Nykypanchuk, D.; Fukuto, M.; Halverson, J. D.; Tkachenko, A. V.; Yager, K. G.; Gang, O. Two-dimensional DNA-programmable assembly of nanoparticles at liquid interfaces. *J. Am. Chem. Soc.* **2014**, *136*, 8323−8332.

(18) Cheng, W.; Campolongo, M. J.; Cha, J. J.; Tan, S. J.; Umbach, C. C.; Muller, D. A.; Luo, D. Free-standing nanoparticle superlattice sheets controlled by DNA. *Nat. Mater.* **2009**, *8*, 519−525.

(19) Ngo, V. A.; Kalia, R. K.; Nakano, A.; Vashishta, P. Supercrystals of DNA-Functionalized Gold Nanoparticles: A Million-Atom Molec-

DOI: 10.1021/acscentsci.6b00170
ACS Cent. Sci. 2016, 2, 614−620

ular Dynamics Simulation Study. *J. Phys. Chem. C* **2012**, *116*, 19579−19585.
(20) Mueggenburg, K. E.; Lin, X.-M.; Goldsmith, R. H.; Jaeger, H. M. Elastic membranes of close-packed nanoparticle arrays. *Nat. Mater.* **2007**, *6*, 656−660.
(21) Wang, Y.; Liao, J.; Mcbride, S. P.; Efrati, E.; Lin, X. M.; Jaeger, H. M. Strong Resistance to Bending Observed for Nanoparticle Membranes. *Nano Lett.* **2015**, *15*, 6732−6737.
(22) Salerno, K. M.; Bolintineanu, D. S.; Lane, J. M. D.; Grest, G. S. High strength, molecularly thin nanoparticle membranes. *Phys. Rev. Lett.* **2014**, *113*, 258301.
(23) Williams, G. A.; Ishige, R.; Cromwell, O. R.; Chung, J.; Takahara, A.; Guan, Z. Mechanically Robust and Self-Healable Superlattice Nanocomposites by Self-Assembly of Single-Component "Sticky" Polymer-Grafted Nanoparticles. *Adv. Mater.* **2015**, *27*, 3934−3941.
(24) Lee, D.; Jia, S.; Banerjee, S.; Bevk, J.; Herman, I. P.; Kysar, J. W. Viscoplastic and granular behavior in films of colloidal nanocrystals. *Phys. Rev. Lett.* **2007**, *98*, 026103.
(25) Lequieu, J. P.; Hinckley, M.; de Pablo, J. J. A molecular view of DNA-conjugated nanoparticle association energies. *Soft Matter* **2015**, *11*, 1919−1929.
(26) Hurst, S. J.; Lytton-Jean, A. K. R.; Mirkin, C. A. Maximizing DNA loading on a range of gold nanoparticle sizes. *Anal. Chem.* **2006**, *78*, 8313−8318.
(27) Rogers, W. B.; Crocker, J. C. Direct measurements of DNA-mediated colloidal interactions and their quantitative modeling. *Proc. Natl. Acad. Sci. U. S. A.* **2011**, *108*, 15687−15692.
(28) Elghanian, R.; Storhoff, J. J.; Mucic, R. C.; Letsinger, R. L.; Mirkin, C. A. Selective Colorimetric Detection of Polynucleotides Based on the Distance-Dependent Optical Properties of Gold Nanoparticles. *Science* **1997**, *277*, 1078−1081.
(29) Audus, D. J.; Starr, F. W.; Douglas, J. F. Coupling of isotropic and directional interactions and its effect on phase separation and self-assembly. *J. Chem. Phys.* **2016**, *144*, 074901.
(30) Li, T.; Sknepnek, R.; Macfarlane, R. J.; Mirkin, C. A.; Olvera de la Cruz, M. Modeling the crystallization of spherical nucleic acid nanoparticle conjugates with molecular dynamics simulations. *Nano Lett.* **2012**, *12*, 2509−2514.
(31) Li, T.; Sknepnek, R.; Olvera de la Cruz, M. Thermally active hybridization drives the crystallization of DNA-functionalized nanoparticles. *J. Am. Chem. Soc.* **2013**, *135*, 8535−8541.
(32) Hinckley, D. M.; Freeman, G. S.; Whitmer, J. K.; de Pablo, J. J. An experimentally-informed coarse-grained 3-site-per-nucleotide model of DNA: Structure, thermodynamics, and dynamics of hybridization. *J. Chem. Phys.* **2013**, *139*, 144903.
(33) Knotts, T. A.; Rathore, N.; Schwartz, D. C.; de Pablo, J. J. A coarse grain model for DNA. *J. Chem. Phys.* **2007**, *126*, 084901.
(34) Sambriski, E. J.; Schwartz, D. C.; de Pablo, J. J. A mesoscale model of DNA and its renaturation. *Biophys. J.* **2009**, *96*, 1675−1690.
(35) Hinckley, D. M.; Lequieu, J. P.; de Pablo, J. J. Coarse-grained modeling of DNA oligomer hybridization: length, sequence, and salt effects. *J. Chem. Phys.* **2014**, *141*, 035102.
(36) Plimpton, S. Fast Parallel Algorithms for Short-Range Molecular Dynamics. *J. Comput. Phys.* **1995**, *117*, 1−19.
(37) Thompson, A. P.; Plimpton, S. J.; Mattson, W. General formulation of pressure and stress tensor for arbitrary many-body interaction potentials under periodic boundary conditions. *J. Chem. Phys.* **2009**, *131*, 154107.

DOI: 10.1021/acscentsci.6b00170
ACS Cent. Sci. 2016, 2, 614−620